



Original scientific paper

Self-assembling nanomaterial-based peptide surface for target cell adhesion

Hasret Turkmen[✉]

Izmir Biomedicine and Genome Center, Balcova 35340, Izmir, Turkey; Department of Biochemistry, Ege University, Izmir, Turkey and Job and Vocational Counselor, Turkish Employment Agency, Izmir, Turkey

Corresponding author: ✉ hasret.turkmen@ibg.edu.tr

Received: January 11, 2023; Accepted: April 7, 2023; Published: April 18, 2023

Abstract

Non-covalent modification of electrode surfaces with nanoparticle-based peptides does not change the chemical properties of the electrode but allows electrochemical measurement of cell adhesion. This study examines the effect of self-modified nanomaterial/peptide surfaces on cell adhesion. This adhesion to the surface is caused by the negative Gibbs free energy formed in the system because of the presence of -OH, sulfur, carbonyl, or reactive groups. A cheaper and more practical method for electrode surfaces targeting cell adhesion, which does not use heavy chemicals and EDC/NHS chemistry, is used in this work. Thanks to the bioactive materials immobilized on the screen-printed carbon electrode (SPCE) surface in a controlled manner and the surface chemistry offered by these materials, a biocompatible self-assembling nanomaterial-based peptide surface platform is created, and cell adhesion is measured by an electrochemical technique. After the characterization steps, electrochemical techniques created a calibration curve of the current value as a function of concentration for each cell line. The adhesion of the generated bioactive electrode surfaces to the selected cell lines was examined comparatively.

Keywords

Screen-printed carbon electrode (SPCE); gold nanoparticles, biofunctionalization; cell lines

Introduction

Non-covalent biofunctionalization of nanoparticles (NPs) is a physical conjugation strategy that can be accomplished through electrostatic, hydrophobic and affinity interactions [1-3]. Both electrostatic and hydrophobic interactions require fewer modification steps, providing a simple, fast, and cost-effective way to biofunctionalized nanoparticles [4]. The adsorption of globular proteins on the negatively charged NPs surface depends on electrostatic interactions. Due to the repulsion between the surface and protein molecules, the maximal adsorption state occurs at the protein isoelectric point

[5,6]. Bioconjugation of NPs with biomolecules through covalent interactions can be accomplished by a simple chemical reaction event through cysteine residues on the surface of biomolecules or using a bifunctional linker [7]. The easiest way to bind biomolecules to gold nanoparticles (AuNPs) is to create weak interactions (electrostatic, hydrophobic, and Van der Waals interactions) between the NPs and the ligand. Thus, proteins self-attach to NPs by adsorption. The surface charge of NPs can be enhanced by ligand functionalization, metal ion binding, or hydrophilic polymer coating. AuNPs can be easily coated with desired ligands by citrate coating, thiol, or amine ligands with higher binding affinity immediately after reduction or by ligand exchange [8-11]. The hydrophobicity, size, radius, and surface coatings of NPs significantly affect NP-cell interactions [12]. The main advantages of these materials are high surface area, improved signal-to-noise ratio, catalytic activity, higher selectivity, and convergent diffusion mode [13]. The therapeutic uses of cell-penetrating cationic, hydrophobic, or amphipathic peptides are common due to their cell targeting and transduction properties.

Cationic peptides such as arginine, lysine, or histidine act independently of the receptor by interacting electrostatically with negatively charged phosphates and sulfates on the plasma membrane, and the partial protonation of the amino groups of histidine makes the peptides in this group the most effective in carrier-cell interaction [14,15]. Moreover, amino acids with aliphatic and aromatic hydrophobic side chains have a water solubility-reducing effect. Peptides containing acidic and basic groups such as histidine and glutamic acid have been reported to have a water solubility-increasing effect [16]. The thiol group, which acts as a reducing agent *in vivo*, breaks disulfide bonds in proteins to yield free cysteine groups [17,18]. Glutathione (GSH) is involved in many biological processes, including metabolism, protein and DNA synthesis, and maintenance of cells [17]. Tang *et al.* developed an electrochemical immunosensor by adding CEA antibodies (CEAAb) to GSH monolayer-modified AuNPs [19]. Similarly, Rusling *et al.* used GSH-conjugated AuNPs and magnetic nanoparticles (MNPs) for the detection of PSA [20]. Sun *et al.* used an electrochemical desorption method to effectively release HepG2 tumor cells by cleaving Au-S bonds at SPGE (surface-imprinted gold electrode) interfaces to selectively capture and isolate cancer cells [21]. Han *et al.* reported that a layer of GSH self-assembles into gold-plated NPs and serves as a binding site through hydrogen bond interactions [22]. Since AuNPs are highly reactive toward the thiol group, they form Au-S bonds with superior affinity [23]. In another study, it was reported that the adsorption of proteins with cysteine residues occurs through a single-point interaction of thiol-derived protein on the AuNP surface, while adsorption of proteins without cysteine residues occurs through non-specific multipoint binding of the protein [24]. It is known that the imidazole ring has a metallic bonding affinity [25]. Dipeptide L-carnosine (Car) has a broad biological activity and has antioxidant (antiglycation) effects, especially for carbohydrates and products on lipids (antioxidation) [26]. The presence of the β -alanine (β AH) residue allows it to react directly with oxidized carbohydrates and lipids, while the histidine (H) residue has been reported to bind to transition metal ions [26]. Another study reported the use of L-carnosine and AuNPs to image HeLa cells [27]. It has been reported that the conductivity of iron oxide nanoparticles is increased due to covalent binding and synthesis with L-carnosine, making it applicable in cell separation, diagnosis, and targeted drug delivery for cancer therapy [28]. It has been reported that carnosine inhibits cancer cell growth by up to 23 % and increases reactive oxygen species (ROS) levels to 30 and 31 % in MDCK and HeLa cells [29]. It has been reported that it inhibits the growth of cancerous cells and shows chaperone activity and anticancer activity by killing transformed cells [30]. Also, it has been reported that the imidazole ring can bind to Au in many ways [31]. Insulin-like growth hormone (IGF-1), which is very similar to insulin, is a basic peptide [32] consisting of 70 amino acids belonging to the tyrosine kinase receptor

family, and having a molecular weight of about 7.5 kDa. It is rich in cysteine and these proteins have important roles in carbohydrate metabolism [33]. Studies have shown that IGF-1 inhibits proliferation and apoptosis and is measured as a biomarker. It was shown that IGF-1 stimulates IL-8 expression in DU-145 (prostate cancer cell line) cells by increasing the transcriptional activity of IGF-1, which has an important role in cancer cells [34]. Some studies have reported that the IGF-1 system is also associated with diabetes and that insulin therapy causes changes in the IGF system [35]. IGF-1 immunosensor was made by immobilizing IGF-1-specific antibodies on gold nanoparticles prepared on the gold electrode surface [36]. IGF-1 receptor (IGF-1R) is overexpressed in lung cancer (A549) and cancer cell proliferation and contributes to malignant transformation and poor prognosis, especially in patients with lung cancer [37]. Many studies have shown that IGF-1 and ROS play a role in the development and progression of various cancers. The already presented research concluded that cancer cells (HeLa, HepG2, and SW1116) and healthy cells (NCM-460) were treated with different concentrations of IGF-1 and that, at other times, cancer cells produced large amounts of cytoplasmic ROS but were not healthy cells. Further mechanistic analyzes showed that IGF-1 activates NF κ B and NLRP3 inflammatory signaling in HeLa cells. Systematic analysis showed that IGF-1 activates NF κ B and NLRP3 and activation depends on cytosolic ROS- and NADPH oxidase 2 (NOX2) [38].

In this study, AuNPs attached to the screen-printed carbon electrode (SPCE) surface by adsorption, and selected peptides (L-glutathione, L-carnosine, and insulin-like growth factor-1) were immobilized on the AuNP-modified surface under optimum conditions. Thus, nanoparticle-based peptide bioconjugates have formed an electroactive region on the electrode surface. Thanks to this self-assembling binding strategy, non-specific adsorption of electroactive surfaces was prevented. Characterization studies of AuNP/peptide-modified SPCE were carried out using electrochemical and spectroscopic methods to analyze the changes in the chemical and physical structure of the modified SPCE surface. After the addition of cancer (U87, A549 and HeLa) and healthy (Vero) cell lines, the interactions of the immobilized electroactive surface and added cells were investigated using electrochemical techniques. A calibration curve of the current value as a function of the concentration of cells was generated for each cell line [39]. Thus, the adhesion behavior of the selected cells to the modified surface was examined mutually. The concentration range in which the current difference was found is directly proportional to the concentration of the analyte on the electrode surface. Thus, an important step was realized for the accurate detection of the target samples.

The originality of this article is primarily based on the absence of similar studies in the literature on the ability to induce cell adhesion for insulin-like growth factor-1, which binds to the gold nanomaterial on the electrode surface. Note that real-time measurement of point-of-care tests (POCTs) through the functionalization of disposable modified electrode surfaces may be useful in their dissemination and diversification.

Experimental

Methods and reagents

L-glutathione (GSH) reduced, L-carnosine (Car) (1 mg/mL) and insulin-like growth factor-1 (IGF-1; 10 mg/mL) were prepared in phosphate buffer (PBS), gold nanoparticles (40 nm diameter, OD 1, stabilized suspension in 0.1 mM PBS, reactant free) were purchased from Sigma-Aldrich chemical company (St. Louis, MO, USA.) and screen-printed carbon electrode (SPCE, DRP-110, 4 mm diameter) were purchased from MetrohmDropsens company. 5.0 mM solution of potassium hexacyanoferrate (HCF) (III) ($K_3Fe(CN)_6$) /potassium hexacyanoferrate (HCF) (II) trihydrate ($K_4Fe(CN)_6 \cdot 3H_2O$) redox couple was prepared in phosphate (pH 7.4) buffer containing 0.1 M KCl solution. Sodium

phosphate buffer (50 mM, pH 7.4) and phosphate-buffered saline (PBS; pH 7.4, 1x) were used as the working buffer solutions. Human lung carcinoma cell line (A549, ATCC, USA), human brain glioblastoma cell line (U87 MG, ATCC, USA), human cervical adenocarcinoma cell line (HeLa, ATCC, USA), and African green monkey normal kidney cell line (Vero, ATCC, USA) were used in experiments. Cells were cultured in a humidified medium at 37 °C in a 5 % CO₂ incubator atmosphere. Culture medium Eagle's Minimum Essential Medium (EMEM, M4655, Merck, USA), supplemented with 10 vol.% fetal bovine serum (FBS, Biowest, France), 1 mM sodium pyruvate (S8636, Sigma, USA), 2 mM L-Glutamine (K0283, Biochrom, Germany) and 100 units/mL penicillin and 100 µg/mL streptomycin (A2213, Biochrom, Germany). The culture medium was replaced with fresh medium every other day and cells were incubated until the desired cell number was reached. Cells separated from each other in tissue culture dishes with trypsin-EDTA solution (0.05 % trypsin, 0.02 % EDTA, Sigma-Aldrich, USA). Scanning electron microscopy (SEM)/energy-dispersive X-ray spectroscopy (EDS) and X-ray photoelectron spectroscopy (XPS) analyses and cell culture studies were performed with standardized methods by Ege University Test and Analysis Laboratory Application and Research Center (EGEMATAL). Thermo Scientific Apreo S brand device was used for SEM/EDS technique and the Thermo Scientific K-Alpha brand device was used for the XPS technique. For differential pulse voltammetry (DPV) and cyclic voltammetry (CV) measurements, PalmSense potentiostat (Palm Instruments, Houten, Netherlands) PS Trace 5.5 program and CHI 6004 C (CH Instruments Incorporated, Austin, TX, USA) devices were used to take EIS measurements.

No electrochemical signal change was observed when the prepared modified electrodes were stored in a closed container at 4 °C for 10 days. All electrochemical experiments were performed on the surface of a screen-printed carbon electrode (SPCE; Dropsense DRP110; overall dimensions: 3.4×1.0×0.05 cm) containing an Ag/AgCl reference electrode, a silver counter electrode and a carbon working electrode. The electrochemical cell placed on a ceramic substrate consists of a three-electrode electrochemical system. All electrochemical experiments were performed in the presence of a redox probe (75 µl) dropped on the surface of the SPCE working electrode. In addition, using the solution prepared to drop on the surface of the SPCE working electrode can reduce the difficulty and cost of electrode fabrication. Measurements were taken using the differential pulse voltammetry (DPV) technique and cyclic voltammetry (CV) technique in the 0.4 V - 0.7 V potential range. The impedance (EIS) measurement was performed at an interference frequency range of 100 kHz ~ 10 mHz and an alternating potential amplitude of 5 mV. By impedance data analysis, ohmic internal resistance, charge transfer internal resistance and diffusion internal resistance were obtained. All measurements were performed in 50 mM phosphate buffer (pH 7.4) containing 5.0 mM Fe(CN)₆^{3-/4-} and 0.1 M KCl solution.

Immobilization of SPCE surfaces

Before the SPCE modification process steps, the SPCE was dipped in distilled H₂O, followed by activation. After washing the SPCE, AuNP (2 µL) was evenly dropped onto the surface of the SPCE working electrode and left for 1 hour in a closed, dark environment. Thus, the physical adsorption of AuNPs took place on the SPCE surface. After drying, the peptide solution (GSH, 4 µL) was dropped onto the electrode. The same procedures were applied to another SPCE surface, this time, the same processes were applied to the electrode surface for Car (4 µl) and IGF-1 (4 µl) instead of GSH. Peptides immobilized to self-assemble on the AuNP-modified SPCE surface were kept in a closed and dark environment overnight. HeLa, U87, Vero, and A549 (prepared in PBS, cell lines 10 and 10⁵ cell concentration, 5 µl) were dropped onto modified SPCE and incubated at 37 °C for 30 minutes.

SEM/EDS and XPS analyses were performed to obtain information about the morphology and chemical structure of the nanomaterial/peptide formed on the SPCE surface in EGEMATAL. Measurements were taken using DPV, CV and EIS techniques. Linearity was determined by calculating the logarithm of the x (number of cells) and y (current difference) axes results for cell adhesion.

Results and discussion

Spectroscopic characterization

X-ray photoelectron spectroscopy (XPS) survey peaks to analyze the changes in the chemical and physical structure of the prepared bio-functional SPCE surfaces are given in Figure 1 [39-43]. To obtain information about the morphological conditions of the prepared bio-functional SPCE surfaces, SEM images of prepared surfaces are given in Figure 2 for blank SPCE surface, SPCE surface after AuNP adsorption and SPCE surface after AuNP/GSH immobilization, SPCE surface after AuNP/Car immobilization, and SPCE surface after AuNP/IGF-1 immobilization.

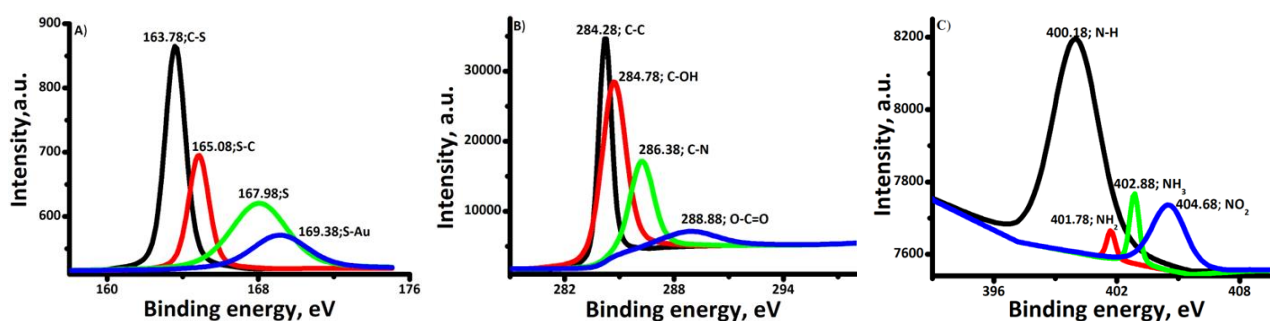


Figure 1. X-ray photoelectron spectroscopy (XPS) survey peaks: A) AuNP/GSH immobilization; S 2p peaks; B) AuNP/Car immobilization; C) AuNP/IGF-1 immobilization; N 1s peaks

Electrochemical characterizations

Potentials applied after functionalization on the electrode surfaces cause conformational changes in peptides due to electrostatic attraction [44]. The resulting biofunctional surfaces resist adhesion under negative potential while they act toward increasing adhesion under positive potential [44]. Electrochemical characterization was performed to evaluate how the ohmic and charge transfer resistance changed. The electrochemical characterization of the modified surfaces is given in Figure 3. In this section, CV, DPV and EIS measurements were analyzed [45]. All these measurements are complementary to each other and present a modification of the surface. When DPV measurements of SPCE in the presence of $\text{Fe}(\text{CN})_6^{3-/4-}$ were examined, the peak current decreased from 27.08 to 19.05 μA after AuNP/GSH modification, from 29.04 to 25.20 μA after AuNP/Car modification, and from 28.22 to 20.37 μA after AuNP/IGF-1 modification of the electrode. Nyquist diagrams of EIS spectra of different modified electrode layers are shown in Figure 3. The high to medium-frequency semicircular segments of each impedance spectrum are due to the $\text{Fe}(\text{CN})_6^{3-/4-}$ electron transfer process. The linear portion of each impedance spectrum appearing at low frequencies is diffusion dependent. Also, the $\text{Fe}(\text{CN})_6^{3-/4-}$ (redox probe) on the electrode surface clarifies the electron transfer kinetics. An increase in the semicircular diameter indicates an increase in electron transfer resistance. The DPV results are in concordance with EIS results. The obtained results of EIS and DPV strongly support each other. These reductions of current in DPV measurements on the electrode surface after the modification processes are proof of successful immobilization on the surface.

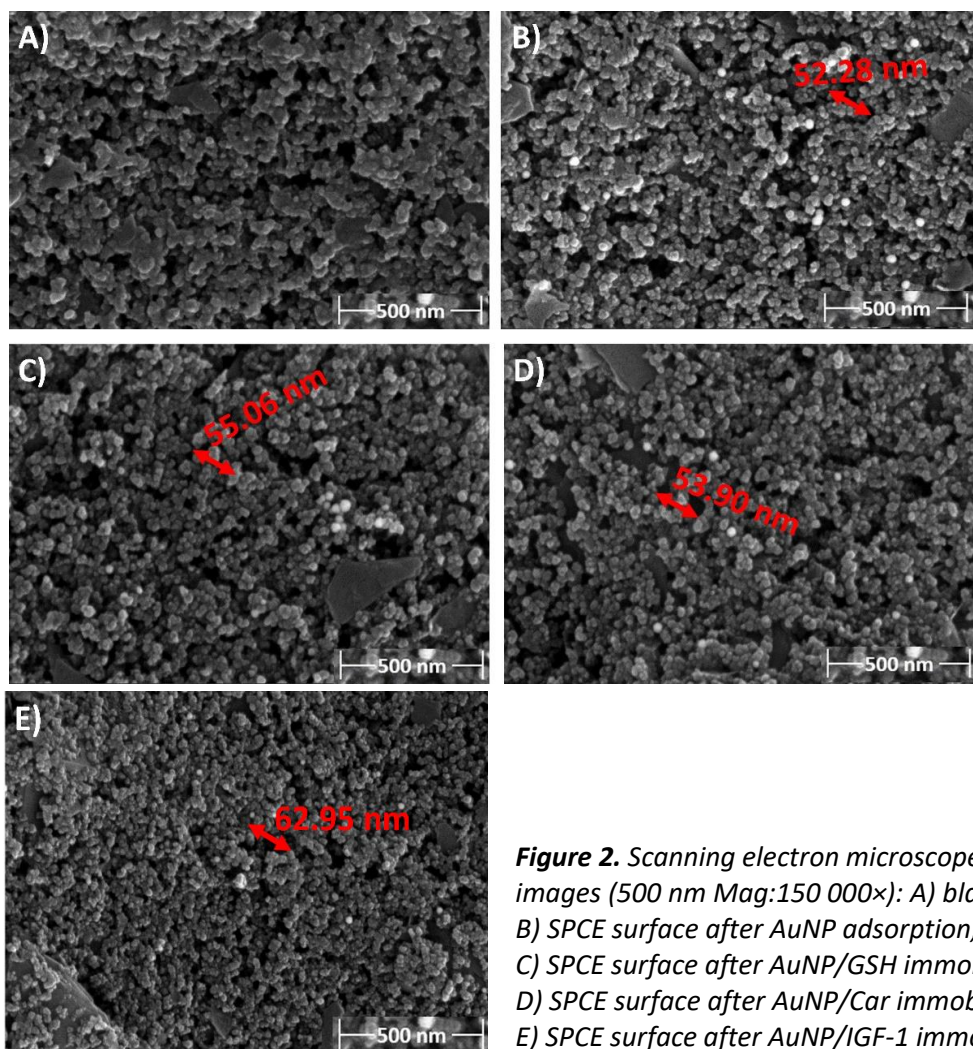


Figure 2. Scanning electron microscope (SEM) images (500 nm Mag:150 000×): A) blank SPCE, B) SPCE surface after AuNP adsorption, C) SPCE surface after AuNP/GSH immobilization, D) SPCE surface after AuNP/Car immobilization, E) SPCE surface after AuNP/IGF-1 immobilization

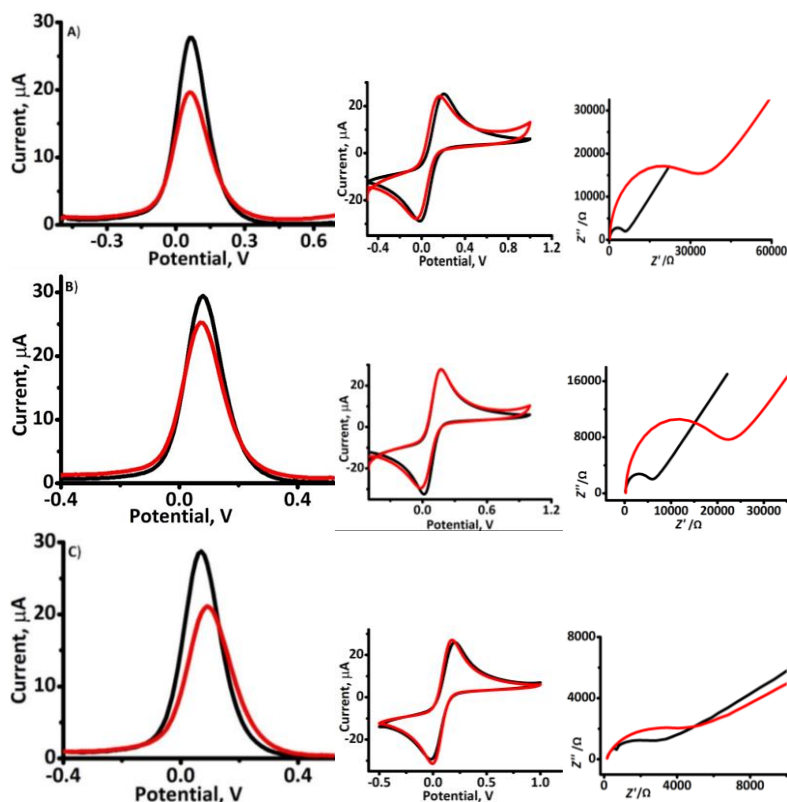


Figure 3. Characterization of modified SPCE surfaces by electrochemical (DPV, CV and EIS) methods: A) AuNP/GSH@SPCE, B) AuNP/Car@SPCE C) AuNP/IGF-1@SPCE. (Black: blank SPCE; Red: AuNP/peptide)

In CV measurements, a slight decrease in anodic and cathodic peaks was observed between the modified and blank electrodes. The decrease in peak current or an increase in the diameter of the semicircle revealed that electron transfer was inhibited. The inhibition of electron transfer is due to insufficient electrochemical communication between the electrode and the modified surface. Also, the diffusion layer may thicken after immobilization.

Adhesion and linear detection range of selected cell lines

After modifications of electrodes, cell adhesions were performed for the targeted cell lines under specified conditions, and a decrease in DPV peak currents was observed. DPV measurements were taken to determine the linear detection range for cancer (U87, A549 and HeLa) and healthy (Vero) cell types after bio-functionalization of the electrode surface (SPCE) with AuNP/GSH, AuNP/Car, and AuNP/IGF-1. For this purpose, cell numbers between 10 and 10⁶ cells/mL were used, each cell type had at least 10 replicates [39]. The current value vs. cell concentration function is, for every modified electrode, which produced a linear response in some remarkable region of cell concentrations, shown in Figure 4. Standard calibration plots that resulted from differences in peak currents observed with increasing cell concentration (cell number per mL) are presented in the insets of Figure 4, together with corresponding linear equations and correlation coefficients (R^2), which are also collected in Table 1.

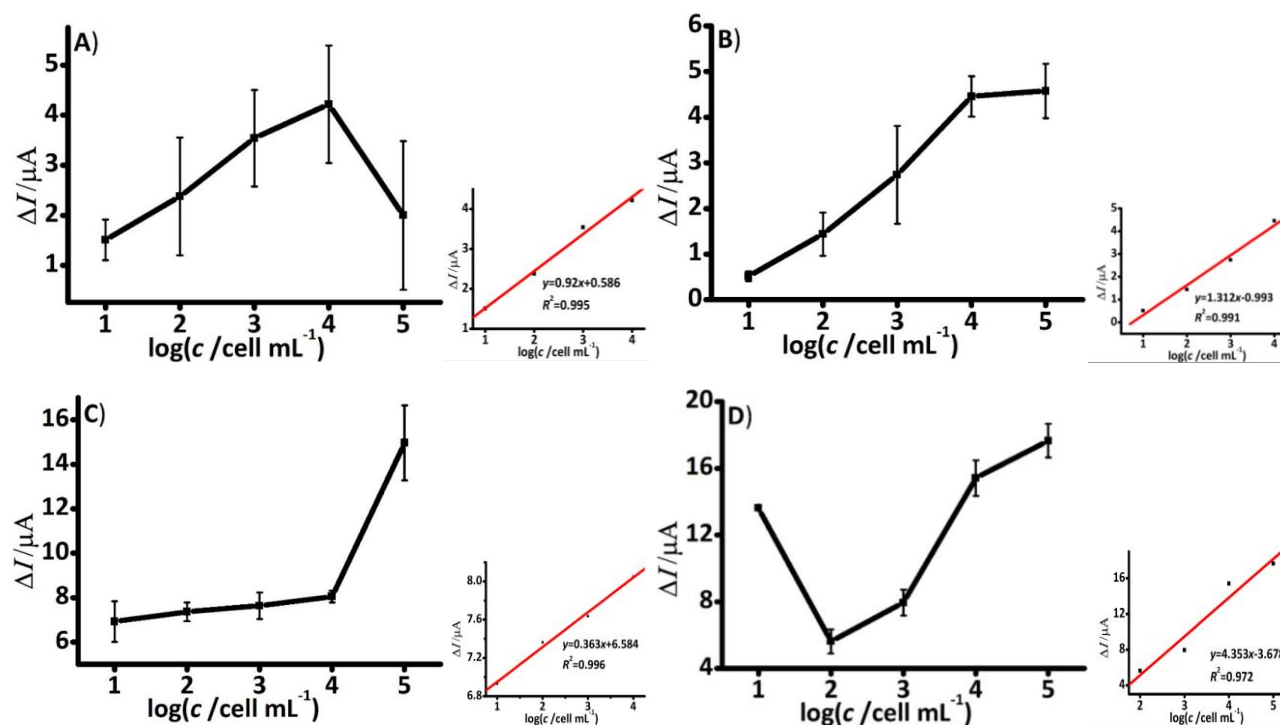


Figure 4. Cell adhesion for modified electrodes: A) AuNP/GSH@SPCE linear standard graphic for the HeLa cell line; B) AuNP/GSH@SPCE linear standard graphic for the U87 cell line; C) AuNP/Car@SPCE linear standard graphic for the A549 cell line; D) AuNP/Car@SPCE linear standard graphic for the HeLa cell line

Electroactive surfaces created using nanomaterial-based peptides to target cells offer researchers privileged opportunities. Peptide-based surfaces support the attachment of cells to extracellular structures (extracellular matrix/ECM). The system must work for a molecule to have a high adsorption capacity. For the system to work, it must have a large surface area, or in other words, the free enthalpy of adsorption (ΔH) and surface free entropy (ΔS) always points in the negative direction. These interfaces between electrodes and modified electrode surfaces are widely used in biotechnology, therapy, diagnosis (diagnosis), and medical applications. In the created system, AuNPs were firstly attached to the SPCE surface that is negatively charged thanks to its carboxyl ends by adsorption and

then functionalized with GSH, Car, and IGF-1. GSH, at pH 7.4. Thanks to the cysteine residues in its structure, GSH has a direct affinity and binding to gold nanoparticles. The system creates a nucleophile structure. Since it has free radicals, the system reacts directly and non-enzymatically, and cysteines (reduces oxidation) directly affect the cellular redox potential. Thanks to the imidazole group in its structure, Car acts as a metal-chelating agent and can easily bind to metal nanoparticles. The affinity of the imidazole group in the Car structure to the Au metal came into play here and functioned as a chelating agent [25]. Disulfide bonds between two cysteine residues form a cyclic region within the IGF-1 molecule. Therefore, it can serve as both a diagnostic biomarker and a therapeutic target.

When the XPS spectra are examined, the N1 nitrogen peak at 400 eV demonstrates the presence of a covalent peptide bond at the surface. It has been reported that all these data play an active role in cellular experiments, with the binding energy of aromatic carbons (C-C) 284.28 eV and the binding energy of C-OH bonds 284-285 eV in C 1s spectra and 286.38 eV binding energy C-O/N, 288.98 eV binding energy O=C=O shows the characteristic peaks [41,46]. N 1s, the binding energy of 400.18 eV-N-H, and the binding energy of 402.88 eV N-H show characteristic peaks. The binding peak of 404.68 eV is due to nitrites. It is also consistent with the data of other researchers [40]. The binding energy of 163.78 eV in S 2p indicates thiol-bound gold. The low binding energies may be due to a charge transfer or the formation of a gold-thiolate bond. It is frequently encountered in XPS simplified sources where the binding energy of 163.78 eV is due to the thiol bond, and the binding energy of 169.38 eV is the metal sulfate bond, the gold-S bond. The XPS data in Figure 1A proves that GSH was successfully attached to SPCE surfaces with AuNP, which agrees with previous studies and retains its chemical structure. When the XPS spectra (Figure 1B) survey of Car is examined, it is seen that the N 1s nitrogen peak, which occurs at 400 eV, forms a covalent peptide bond on the surface, and this data plays an active role in cellular experiments. The C 1s component was 284.8 eV (C-C in aromatic rings), 286.38 eV (C-O), and 288.9 eV (O=C=O), while C-N (amine) and N-C=O (amide in the imidazole ring of carnosine) two new peaks appeared at 286.38 and 289.8 eV, respectively. It was concluded that the imidazole ring in the Car structure made metallic bonds with AuNP. The imidazole ring of carnosine is a cyclopentadiene structure with a non-contiguous CH group (N3 and N1 regions) replaced by N and NH, and it has been reported that it makes a strong bond with a lone electron pair from the N3 region with gold [31]. It has been reported that the imidazole ring can be attached to Au in many ways, and complexes with a single Au atom prefer two imidazole rings, while complexes with 2 or 3 Au atoms prefer three imidazole rings [31]. XPS spectra (Figure 1C) showed that the nitrogen peak at 400 eV is characteristic. It has been reported that if an N1s peak below 400 eV occurs, or if these peaks did not occur, it could be said that IGF-1 was bound by adsorption to the surface as an easily diffused unstable bioactive molecule [44]. Therefore, it suggests that the cysteine residues in its structure are attached not by adsorption but by its affinity for AuNP. It is a characteristic peak of 400 eV, and it has been stated that it is a peptide bond peak and is covalently bound to the surface [43].

Morphological characterization and comparative SEM images of the bifunctional surfaces formed with AuNP/peptide on the SPCE surface and the empty SPCE surface are shown in Figure 2. The particle diameters of the created SPCE surface are between 35.61 and 45.39 nm for the blank SPCE (Figure 2A), while the diameters of particles after AuNP adsorption were between 41.09 and 52.28 nm (Figure 2B). The diameters of the SPCE surface particles after AuNP/GSH immobilization were between 48.42 and 55.06 nm (Figure 2C). After AuNP/Car immobilization, the diameter of the SPCE surface is between 47.52 and 53.90 nm (Figure 2D), while after AuNP/IGF-1 immobilization, the diameter of particles is between 45.86 and 62.95 nm (Figure 2E). Generally, SEM analysis showed

that the surface particle diameter increased as the surface was successfully modified, showing the aggregate formation and homogeneous distribution of particles on the surface.

Differential pulse voltammetry (DPV) measurements were performed to examine the redox properties of modified SPCE electrodes, CV to show the electroactivity and modification of the formed surface, and EIS measurements for the interfacial properties of molecules on the surfaces during immobilization were performed with at least 10 replications, respectively [47]. The compatibility of these different measurements with each other indicates that the surface has been modified (Figure 3). Looking at DPV currents, the diffusion layer has thickened, and studies have shown that the decrease in the oxidation peak current is due to a lack of establishing electrochemical communication between the electrode and the modified surface because of the inhibition of electron transfer [48,49]. The changes in the peak potentials between the blank SPCE and the modified electrode suggest that the surface was changed and the electron transfer rate on the surface was also changed, proving that the surface was successfully modified [50]. Impedance (EIS) studies have shown that electrode immobilization with inorganic NPs, gold nanoparticles [51], or silver nanoparticles [52], significantly reduces charge transfer resistance. DPV measurements, CV measurements and EIS measurements provide information as evidence for surface immobilization. The bioconjugate surface formed has been functionalized in a controlled manner. Surface functional groups such as carboxyl (COOH) and hydroxyl (OH) form integrin bonds with cell ligands. Hydroxyl and carboxyl groups on the surface potentially form hydrogen bonds with cell surface lipids and ions, and higher surface energy leads to the formation of much stronger cell-ligand bonds. Also, the partial positive result of the O=C-N nitrogen atom is proven in XPS data. The charge on the oxygen atom and the partial negative charge form a dipole and hydrogen bonds with the lower phase molecules, and cell-substrate interaction occurs. Since van der Waals and electrostatic interactions, and hence cell-surface interaction, affect the surface energy of the bioactive surface created, surface energy also affects cell adhesion. Thanks to this interaction, any non-specific cell adsorption is prevented.

For the adhesion of the selected cell lines, the linear detection range for cells was established by the change of peak current values observed for modified electrodes with respect to the log of the cell concentration (cell number/mL) obtained by DPV analysis (Figure 4). Differences in peak current values with increasing cell concentrations per mL were obtained as a function of the cell number selected on surfaces. When current difference versus log (cell/mL) graphs are plotted, the correlation coefficient (R^2) was calculated in the linear regression analysis for modified surfaces (Table 1). Although the surfaces prepared, as seen in DPV measurements with various cell lines, provide cell adhesion, standard graphs were created to understand whether the standard graphs of data obtained from these surfaces were linear. For linearity, the difference of current values was taken on the y-axis, while the logarithms of cell concentrations were taken on the x-axis, and graphs were created (Figure 4). VERO was used as a control group in this study. All modified surfaces were used, and cell incubation was performed under the same conditions. Between all modified electrodes treated here, however, some surfaces showed a linear response, but some did not (Table 1).

Table 1. Linear equations and correlation coefficients of calibration plots for selected cell lines

Modified SPCE	HeLa cell line	U87 cell line	A549 cell line	Vero cell line
AuNP/GSH@SPCE	$R^2=0.995$ $y=0.92x+0.586$	$R^2=0.991$ $y=1.312x-0.99$	-	-
AuNP/IGF-1@SPCE	-	-	-	-
AuNP/Car@SPCE	$R^2=0.972$ $y=4.353x-3.68$	-	$R^2=0.996$ $y=0.363x+6.584$	-

Although the resistance of the bioconjugates formed on the SPCE surface to electron transfer causes its conductivity to decrease, its response to cell adhesion indicates that it maintains its

conductivity. Thanks to the equations of the calibration graphs, the cell concentrations were increased per mL and the change in the resistance applied by the cell membrane to the bio-functional surface was observed. Thanks to the linear detection equations of the calibration charts, the targeted cells can be accurately detected. For AuNP/GSH@SPCE, a linear range of up to 10 to 10⁴ cells/mL was obtained in HeLa and U87 cell lines. Although adhesion was observed for Vero and A549 cell lines, a linear range could not be obtained. For AuNP/Car@SPCE, a linear range of 10 to 10⁴ cells/mL was obtained for A549 and 100 to 10⁵ cells/mL for HeLa cell lines. Although adhesion was observed for Vero and U87 cell lines, no linear range could be obtained. For AuNP/IGF-1@SPCE, adhesion was obtained for all selected cells but not a linear range. This may be caused by steric hindrance on the electrode surface due to its high molecular weight. IGF-1 can be used as a biomarker that detects cancer cells, optimization studies are carried out thanks to its excellent nature and the bioconjugate it forms with AuNP.

Conclusion

In this study, conductive-bifunctional surfaces that can be used for cell adhesion are prepared. It was shown that successful electrode surface modification could eventually result from a cancer diagnostic sensor for detecting selective cancer cells.

The surfaces of SPCE were modified with AuNP/GSH, AuNP/Car, and AuNP/IGF-1 and used as a basis for targeted cancer diagnosis sensors. Thanks to the topographical interaction between gold nanostructures and peptide imprinted surfaces, microscale concave structures created a suitable surface area for the adhesion of target cells. Therefore, this study could be considered a pioneer work in recognizing specific cell surfaces.

This work demonstrates that the AuNP/peptide monolayer mounted on the SPCE surface promotes cell adhesion. The gold nanoparticles were assembled on the SPCE, which increases the electrode surface, makes covalent bonds with peptides, and enhances cell adhesion properties. Functional interfaces of selected AuNP/peptides indicate cell adhesion even if they are not RGD peptides or combinations. However, it is unclear whether the adhesion to the cell is due to the combination of carbon material, AuNP, or the selected peptide. In the future direction, the study allows it to be used in point-of-care (POC) studies.

The results of this study demonstrate that nanomaterial-based peptides are important in cell targeting and cell differentiation. The success of the disposable NP/peptide electrode surface, which is created with a simple method without heavy chemicals and at a lower cost, in the study allows it to be used for biomedical applications. In the future, it may pave the way for personalized sensor applications IoT-connected to detect cancer cell lines. In addition, we will integrate blockchain technology, a decentralized technology, into sensor-IoT-based architectures for the traceability and security of the obtained data.

Acknowledgements: *The author would like to thank the editors and anonymous reviewers for providing insightful suggestions and comments to improve the quality of the research paper. Also, I would like to thank my professors, Figen ZIHNIUGLU, Suna TIMUR, and Dilek DEMIRKOL, for their help during my PhD studies.*

References

- [1] J. Yu, M. L. Becker, G. A. Carri, The influence of Amino Acid Sequence and Functionality on the Binding Process of Peptides onto Gold Surfaces, *Langmuir* **28(2)** (2012) 1408-1417. <https://doi.org/10.1021/la204109r>

- [2] C. M. Niemeyer, Nanoparticles, Proteins, and Nucleic Acids: Biotechnology Meets Materials Science, *Angewandte Chemie International Edition* **40(22)** (2001) 4128-4158. [https://doi.org/10.1002/1521-3773\(20011119\)40:22<4128::AID-ANIE4128>3.0.CO;2-S](https://doi.org/10.1002/1521-3773(20011119)40:22<4128::AID-ANIE4128>3.0.CO;2-S)
- [3] S. Tatematsu, T. Ohnishi, S. Saito, M. Tanaka, Y. Hayamizu, M. Okochi, Assemblies of Bi-functional Peptides on Pyrolytic Graphite for Cell Adhesion, *Biochemical Engineering Journal* **170** (2021) 107988. <https://doi.org/10.1016/j.bej.2021.107988>
- [4] Y. Zhang, R. Huang, X. Zhu, L. Wang, C. Wu, Synthesis, Properties, and Optical Applications of Noble Metal Nanoparticle-Biomolecule Conjugates, *Chinese Science Bulletin* **57(2)** (2012) 238-246. <https://doi.org/10.1007/s11434-011-4747-x>
- [5] J. Meissner, A. Prause, B. Bharti, G.H. Findenegg, Characterization of Protein Adsorption onto Silica Nanoparticles: Influence of pH and Ionic Strength, *Colloid and Polymer Science* **293**(2015) 3381- 3391. <https://doi.org/10.1007/s00396-015-3754-x>
- [6] H. K. Chan, P. C. L. Kwok, Production Methods for Nanodrug Particles Using the Bottom-up Approach, *Advanced Drug Delivery Reviews* **63(6)** (2011) 406-416. <https://doi.org/10.1016/j.addr.2011.03.011>
- [7] M. De, P.S. Ghosh, V.M. Rotello, Applications of Nanoparticles in Biology, *Advanced Materials* **20(22)** (2008) 4225-4241. <https://doi.org/10.1002/adma.200703183>
- [8] R. S. Ingram, M. J. Hostetler, R. W. Murray, Poly-Hetero- Ω -Functionalized Alkanethiolate-Stabilized Gold Cluster Compounds, *Journal of the American Chemical Society* **119(39)** (1997) 9175-9178. <https://doi.org/10.1021/ja971734n>
- [9] A. C. Templeton, W. P. Wuelfing, R. W. Murray, Monolayer-Protected Cluster Molecules, *Accounts of Chemical Research* **33(1)** (2000) 27-36. <https://doi.org/10.1021/ar9602664>
- [10] F. Porta, G. Speranza, Ž. Krpetić, V. Dal Santo, P. Francescato, G. Scari, Gold Nanoparticles Capped By Peptides, *Materials Science and Engineering: B* **140(3)** (2007) 187-194. <https://doi.org/10.1016/j.mseb.2007.03.019>
- [11] C. L. Chen, P. Zhang, N. L. Rosi, A New Peptide-Based Method for The Design and Synthesis of Nanoparticle Superstructures: Construction of Highly Ordered Gold Nanoparticle Double Helices, *Journal of the American Chemical Society* **130(41)** (2008) 13555-13557. <https://doi.org/10.1021/ja805683r>
- [12] Y. Sun, Y. Luo, L. Sun, X.-R. Wang, L.-W. Chen, N. Zhang, Y. Wang, L.-Y. Dong, H. Guo, X.-H. Wang, Improving Performance of Cell Imprinted PDMS by Integrating Boronate Affinity and Local Post-Imprinting Modification for Selective Capture of Circulating Tumor Cells From Cancer Patients, *Biosensors and Bioelectronics* **223** (2023) 115023. <https://doi.org/10.1016/j.bios.2022.115023>
- [13] C. M. Welch, R. G. Compton, The Use of Nanoparticles in Electroanalysis, *Analytical and Bio-analytical Chemistry* **384(3)** (2006) 601-619. <https://doi.org/10.1007/s00216-005-0230-3>
- [14] A. Bolhassani, Potential Efficacy Of Cell-Penetrating Peptides for Nucleic Acid and Drug Delivery in Cancer, *Biochimica et Biophysica Acta (BBA)-Reviews on Cancer* **1816(2)** (2011) 232-246. <https://doi.org/10.1016/j.bbcan.2011.07.006>
- [15] E. Koren, V. P. Torchilin, Cell-Penetrating Peptides: Breaking Through to the Other Side, *Trends in Molecular Medicine* **18(7)** (2012) 385-393. <https://doi.org/10.1016/j.molmed.2012.04.012>
- [16] S. Pacheco, T. Kanou, S. Y. Fung, K. Chen, D. Lee, X. Bai, S. Keshavjee, M. Liu, Formulation of Hydrophobic Therapeutics with Self-Assembling Peptide and Amino Acid: A New Platform for Intravenous Drug Delivery, *Journal of Controlled Release* **239** (2016) 211-222. <https://doi.org/10.1016/j.jconrel.2016.08.038>
- [17] Q. Ning, Q. Chen, Y. Huang, Y. Wang, Y. Wang & Z. Liu, Development of a Hg²⁺-Stabilized Double-Stranded DNA Probe for Low-Cost Visual Detection of Glutathione in Food Based on

- G-Quadruplex/hemin DNAzymes, *Journal of Analytical Chemistry* **77** (2022) 1517-1525. <https://doi.org/10.1134/S1061934822120103>
- [18] J. Pronk, R. Meulenbergh, W. Hazeu, P. Bos, J. Kuenen, Oxidation of Reduced Inorganic Sulphur Compounds by Acidophilic Thiobacilli, *FEMS Microbiology Letters* **75**(2-3) (1990) 293-306. [https://doi.org/10.1016/0378-1097\(90\)90540-7](https://doi.org/10.1016/0378-1097(90)90540-7)
- [19] H. Tang, J. Chen, L. Nie, Y. Kuang, S. Yao, A Label-Free Electrochemical Immunoassay for Carcinoembryonic antigen (CEA) Based on Gold Nanoparticles (AuNPs) and Nonconductive Polymer Film, *Biosensors and Bioelectronics* **22**(6) (2007) 1061-1067. <https://doi.org/10.1016/j.bios.2006.04.027>
- [20] J. F. Rusling, G. Sotzing, F. Papadimitrakopoulou, Designing Nanomaterial-Enhanced Electrochemical Immunosensors for Cancer Biomarker Proteins, *Bioelectrochemistry* **76**(1-2) (2009) 189-194. <https://doi.org/10.1016/j.bioelechem.2009.03.011>
- [21] D. Sun, J. Lu, D. Chen, Y. Jiang, Z. Wang, W. Qin, Y. Yu, Z. Chen, Y. Zhang, Label-Free Electrochemical Detection of Hepg2 Tumor Cells with a Self-Assembled DNA Nanostructure-Based Aptasensor, *Sensors and Actuators B* **268** (2018) 359-367. <https://doi.org/10.1016/j.snb.2018.04.142>
- [22] Q. Han, X. Shen, W. Zhu, C. Zhu, X. Zhou, H. Jiang, Magnetic Sensing Film Based on Fe₃O₄@Au-GSH Molecularly Imprinted Polymers for The Electrochemical Detection of Estradiol, *Biosensors and Bioelectronics* **79** (2016) 180-186. <https://doi.org/10.1016/j.bios.2015.12.017>
- [23] V. Spampinato, M. A. Parracino, R. La Spina, F. Rossi, G. Ceccone, Surface Analysis of Gold Nanoparticles Functionalized with Thiol-Modified Glucose SAMs for Biosensor Applications, *Frontiers in Chemistry* **4** (2016) 8. <http://dx.doi.org/10.3389/fchem.2016.00008>
- [24] S. H. Mejias, P. Couleaud, S. Casado, D. Granados, M. A. Garcia, J. M. Abad, A. L. Cortajarena, Assembly of Designed Protein Scaffolds into Monolayers for Nanoparticle Patterning, *Colloids and Surfaces B* **141** (2016) 93-101. <https://doi.org/10.1016/j.colsurfb.2016.01.039>
- [25] F. Bellia, G. Vecchio, E. Rizzarelli, Carnosine Derivatives: New Multifunctional Drug-Like Molecules, *Amino Acids* **43**(1) (2012) 153-163. <https://doi.org/10.1007/s00726-011-1178-6>
- [26] I. W. Hamley, Small Bioactive Peptides for Biomaterials Design and Therapeutics, *Chemical Reviews* **117**(24) (2017) 14015-14041. <https://doi.org/10.1021/acs.chemrev.7b00522>
- [27] D. Li, Y. Dong, B. Li, Y. Wu, K. Wang, S. Zhang, Colorimetric Sensor Array with Unmodified Noble Metal Nanoparticles for Naked-Eye Detection of Proteins and Bacteria, *Analyst* **140**(22) (2015) 7672-7677. <https://doi.org/10.1039/C5AN01267H>
- [28] Z. Durmus, H. Kavas, A. Baykal, H. Sozeri, L. Alpsoy, S. Çelik, M. Toprak, Synthesis and Characterization of l-Carnosine Coated Iron Oxide Nanoparticles, *Journal of Alloys and Compounds* **509**(5) (2011) 2555-2561. <https://doi.org/10.1016/j.jallcom.2010.11.088>
- [29] M. Pandurangan, G. Enkhtaivan, D.H. Kim, Therapeutic Efficacy of Natural Dipeptide Carnosine Against Human Cervical Carcinoma Cells, *Journal of Molecular Recognition* **29**(9) (2016) 426-435. <https://doi.org/10.1002/jmr.2541>
- [30] A. R. Hipkiss, Ageing and Carnosine: Are Carnivorous Diets Beneficial?, *Mechanisms of Ageing and Development* **126**(10) (2005) 1034-1039. <https://doi.org/10.1016/j.mad.2005.05.002>
- [31] M. Gatchell, M. Goulart, L. Kranabetter, M. Kuhn, P. Martini, B. Rasul, P. Scheier, P. Scheier, Complexes of Gold and Imidazole Formed in Helium Nanodroplets, *Physical Chemistry Chemical Physics* **20**(11) (2018) 7739-7745. <https://doi.org/10.1039/C8CP00486B>
- [32] D. J. Hill, Relationships of Insulin-Like Growth Factors and Their Binding Proteins to Embryonic Development, *Journal of Animal Science* **74**(suppl_2) (1996) 85-93. https://doi.org/10.2527/1996.74suppl_285x

- [33] J. R. Florini, D. Z. Ewton, S. A. Coolican, Growth Hormone and the Insulin-Like Growth Factor System in Myogenesis, *Endocrine Reviews* **17(5)** (1996) 481-517. <https://doi.org/10.1210/edrv-17-5-481>
- [34] R. Kooijman, E. Himpe, S. Potikanond, A. Coppens, Regulation of Interleukin-8 Expression in Human Prostate Cancer Cells by Insulin-Like Growth Factor-I and Inflammatory Cytokines, *Growth Hormone & IGF Research* **17(5)** (2007) 383-391. <https://doi.org/10.1016/j.ghir.2007.04.004>
- [35] L. A. Bach, M. M. Rechler, The Insulin-like Growth Factor System: Towards Clinical Applications, *Diabetes/Metabolism Reviews* **8(3)** (1992) 229-257. <https://doi.org/10.1002/dmr.5610080304>
- [36] B. Rezaei, N. Majidi, H. Rahmani, T. Khayamian, Electrochemical Impedimetric Immunosensor for Insulin-Like Growth Factor-1 Using Specific Monoclonal Antibody-Nanogold Modified Electrode, *Biosensors and Bioelectronics* **26(5)** (2011) 2130-2134. <https://doi.org/10.1016/j.bios.2010.09.020>
- [37] M. Yin, X. Guan, Z. Liao, Q. Wei, Insulin-Like Growth Factor-1 Receptor-Targeted Therapy for Non-Small Cell Lung Cancer: A Mini Review, *American Journal of Translational Research* **1(2)** (2009) 101. <https://www.ncbi.nlm.nih.gov/pmc/articles/PMC2776317/>
- [38] C. Wang, Y. An, Y. Wang, K. Shen, X. Wang, W. Luan, F. Ma, L. Ni, M. Liu, L. Yu, Insulin-Like Growth Factor-I Activates Nfkb And NLRP3 Inflammatory Signalling Via ROS In Cancer Cells, *Molecular and Cellular Probes* **52** (2020) 101583. <https://doi.org/10.1016/j.mcp.2020.101583>
- [39] J. J. Castillo, W. E. Svendsen, N. Rozlosnik, P. Escobar, F. Martínez, J. Castillo-León, Detection of Cancer Cells Using A Peptidenanotube-Folic Acid Modified Graphene Electrode, *Analyst* **138(4)** (2013) 1026-1031. <https://doi.org/10.1039/C2AN36121C>
- [40] A. Ghahremaninezhad, D. Dixon, E. Asselin, Electrochemical And XPS Analysis Of Chalcopyrite (Cufes₂) Dissolution In Sulfuric Acid Solution, *Electrochimica Acta* **87** (2013) 97-112. <https://doi.org/10.1016/j.electacta.2012.07.119>
- [41] T. Matsukura, T. Takahashi, Y. Nishimura, T. Ohtani, M. Sawada, K. Shibata, Characterization of Crystalline L-Carnosine Zn(II) Complex (Z-103), A Novel Anti-Gastric Ulcer Agent : Tautomeric Change of Imidazole Moiety Upon Complexation, *Chemical and Pharmaceutical Bulletin* **38(11)** (1990) 3140-3146. <https://doi.org/10.1248/cpb.38.3140>
- [42] B. Pelaz, V. Grazu, A. Ibarra, C. Magen, P. del Pino, J.M. de la Fuente, Tailoring the Synthesis and Heating Ability of Gold Nanoprisms for Bioapplications, *Langmuir* **28(24)** (2012) 8965-8970. <https://doi.org/10.1021/la204712u>
- [43] D. Ito, T. Kado, F. Nagano-Takebe, T. Hidaka, K. Endo, Y. Furuichi, Biological Activation of Zirconia Surfaces by Chemical Modification With IGF-1, *Journal of Biomedical Materials Research A* **103(11)** (2015) 3659-3665. <https://doi.org/10.1002/jbm.a.35476>
- [44] L. Zhang, Z. Wang, J. Das, M. Labib, S. Ahmed, E.H. Sargent, S.O. Kelley, Potential-Responsive Surfaces for Manipulation of Cell Adhesion, Release, and Differentiation, *Angewandte Chemie International Edition* **58(41)** (2019) 14519-14523. <https://doi.org/10.1002/anie.201907817>
- [45] J. Yu, P. Zhang, T. Chen, Q. Lv, L. Gao, B. Liu, J. Duan, Z. Wu, J. Li, Construction of Flexible and Wearable 3D TiO₂ NTs@Ti Mesh for Physiological Detection Based on Sweat, *JCIS Open* **2** (2021) 100007. <https://doi.org/10.1016/j.jciso.2021.100007>
- [46] C. Meng, X. Zhi, C. Li, C. Li, Z. Chen, X. Qiu, C. Ding, L. Ma, H. Lu, D. Chen, G. Liu, D. Cui, Graphene Oxides Decorated with Carnosine as an Adjuvant to Modulate Innate Immune and Improve Adaptive Immunity *In Vivo*, *ACS Nano* **10(2)** (2016) 2203-2213. <https://doi.org/10.1021/acsnano.5b06750>

- [47] X. Y. Ge, Y. G. Feng, S. Y. Cen, A. J. Wang, L. P. Mei, X. Luo, J. J. Feng, A Label-Free Electrochemical Immunosensor Based on Signal Magnification of Oxygen Reduction Reaction Catalyzed by Uniform PtCo Nanodendrites for Highly Sensitive Detection of Carbohydrate Antigen 15-3, *Analytica Chimica Acta* **1176** (2021) 338750. <https://doi.org/10.1016/j.aca.2021.338750>
- [48] L. Liu, X. Zhu, D. Zhang, J. Huang, G. Li, An Electrochemical Method to Detect Folate Receptor Positive Tumor Cells, *Electrochemistry Communications* **9**(10) (2007) 2547-2550. <https://doi.org/10.1016/j.elecom.2007.07.032>
- [49] R. Wang, J. Di, J. Ma, Z. Ma, Highly Sensitive Detection Of Cancer Cells By Electrochemical Impedance Spectroscopy, *Electrochimica Acta* **61** (2012) 179-184. <https://doi.org/10.1016/j.electacta.2011.11.112>
- [50] X. Lv, W. Ge, Q. Li, Y. Wu, H. Jiang, X. Wang, Rapid and Ultrasensitive Electrochemical Detection of Multidrug-Resistant Bacteria Based on Nanostructured Gold Coated ITO Electrode, *ACS Applied Materials & Interfaces* **6**(14) (2014) 11025-11031. <https://doi.org/10.1021/am5016099>
- [51] F. Tulli, F. A. Gulotta, D. M. Martino, V. I. P. Zanini, C. D. Borsarelli, Ultrasensitive Amperometric Biosensing of Polyphenols Using Horseradish Peroxidase Immobilized in a Laponite/Au/DNA-Bioinspired Polycation Nanocomposite, *Journal of The Electrochemical Society* **165**(10) (2018) B452. <https://doi.org/10.1149/2.1191810jes>
- [52] S. Sandeep, A. S. Santhosh, N. K. Swamy, G. S. Suresh, J. S. Melo, N. A. Chamaraja, A Biosensor Based on a Graphene Nanoribbon/Silver Nanoparticle/Polyphenol Oxidase Composite Matrix on a Graphite Electrode: Application in the Analysis Of Catechol in Green Tea Samples, *New Journal of Chemistry* **42**(20) (2018) 16620-16629. <https://doi.org/10.1039/C8NJ02325E>